THE SUPERCONVERGENT PATCH RECOVERY AND *A POSTERIORI* ERROR ESTIMATES. PART 2: ERROR ESTIMATES AND ADAPTIVITY

O. C. ZIENKIEWICZ AND J. Z. ZHU

Institute of Numerical Methods in Engineering, University College of Swansea, Singleton Park, Swansea SA2 8PP, U.K.

SUMMARY

In this second part of the paper, the issue of *a posteriori* error estimation is discussed. In particular, we derive a theorem showing the dependence of the effectivity index for the Zienkiewicz–Zhu error estimator on the convergence rate of the recovered solution. This shows that with superconvergent recovery the effectivity index tends asymptotically to unity. The superconvergent recovery technique developed in the first part of the paper[1] is used in the computation of the Zienkiewicz–Zhu error estimator to demonstrate accurate estimation of the exact error attainable. Numerical tests are shown for various element types illustrating the excellent effectivity of the error estimator in the energy norm and pointwise gradient (stress) error estimation. Several examples of the performance of the error estimator in adaptive mesh refinement are also presented.

1. INTRODUCTION

The error estimator developed by the authors (and sometimes known as the Zienkiewicz–Zhu or Z^2 error estimator)[2] has proved to be economical and effective both in evaluating errors simply for a given analysis and as a prelude to adaptive processes. Indeed, it is now widely used in many industrial codes.

The essence of the procedure is to use the difference between the values of the post-processed, recovered, more accurate gradients (stresses) $\boldsymbol{\sigma}^*$ and these given directly by the finite element solution $\boldsymbol{\sigma}_h$ i.e.

$$\mathbf{e}_\sigma^* = \boldsymbol{\sigma}^* - \boldsymbol{\sigma}_h \tag{1}$$

as a measure of the local error. The error can then be evaluated in any appropriate norm defined in terms of derivative errors. Here most frequently the energy norm is used, though other norms can be adopted.

It is obvious that the success of the procedure is dependent on the accuracy of the recovered gradients. The global L_2 projection and simple averaging techniques were originally recommended by the authors but it was soon found that such recovery techniques were inadequate for quadratic approximations. For this reason empirical correction factors were introduced early to increase the computed error values[2] which were always underestimated.

In the first part of the present paper[1] we introduced a highly accurate recovery process with superconvergent properties and obviously its use in the Z^2 error estimator should be highly beneficial. The present paper explores this avenue and shows the extremely accurate estimation of

the actual discretization error which can now be achieved without correction factors, which to many are displeasing.

To demonstrate the relationship between the accuracy of the recovered solution and the effectivity index of the Z^2 error estimator more precisely we introduce in Section 2 of this paper a theorem which shows the bounds of the effectivity index. The same theorem does in fact show that with the superconvergent accuracy of the recovery procedure an asymptotic convergence of the effectivity index to unity is to be expected. Numerical studies on various element types which are then presented indicate the asymptotically exact error estimation achievable in practice.

In most of the examples presented we look at the error in the energy norm. However, other norms could be similarly used. We thus devote a section to numerical studies of local (pointwise) error estimation.

In all the studies here presented we concentrate upon the h refinement process, but of course the improved error estimator is available for all p values and could be effectively used in p or h–p adaptive refinement.

The Z^2 error estimator discussed here is but one of several possibilities for *a posteriori* error estimation. The main alternative is that of evaluating residuals and accomplishing directly a local auxiliary solution to determine the error. This is the basis of the first error estimator derived by Babuska and Rheinboldt[3] and elaborated in detail by others.[4-8] With the accuracy which can be achieved and the economy of implementation of the recovery procedure proposed in Part I,[1] we feel that a near optimal position for the Z^2 error estimator has been now established. The wide applicability of the procedure demonstrated in many studies[9-16] and the ease of coupling with adaptivity augur well for its future.

2. THE Z^2 ERROR ESTIMATOR AND ITS EFFECTIVITY INDEX

In order to illustrate the basic theory, we shall consider the problem of elasticity as a model. The error of the finite element approximation $\mathbf{u}_h$ with respect to the exact solution $\mathbf{u}$ is defined as

$$\mathbf{e} = \mathbf{u} - \mathbf{u}_h \tag{2}$$

and the error of the stresses (gradients) is defined as

$$\mathbf{e}_\sigma = \boldsymbol{\sigma} - \boldsymbol{\sigma}_h \tag{3}$$

The exact solutions $\mathbf{u}$ and $\boldsymbol{\sigma}$ are obviously not available in practical computations. To evaluate the error, we seek therefore some practical and effective method for estimating $\mathbf{e}$ or $\mathbf{e}_\sigma$ in an appropriate norm. We shall in the following use the energy norm of error $\mathbf{e}$ when discussing the basic feature of the *a posteriori* error estimation. However, any other norm can be included here providing this depends on $\mathbf{e}_\sigma$.

The energy norm of $\mathbf{e}$ is written as

$$\| \mathbf{e} \| = \| \mathbf{u} - \mathbf{u}_h \| = \left(\int_\Omega \mathbf{e}_\sigma^{\mathrm{T}} \mathbf{D}^{-1} \mathbf{e}_\sigma \, \mathrm{d}\Omega \right)^{1/2} \tag{4}$$

where Ω is the domain on which the problem is defined and $\mathbf{D}$ is the elasticity matrix. The basic concept of the Zienkiewicz–Zhu error estimator consists of replacing the exact value of $\mathbf{e}_\sigma$ in equation (3) or (4) by an approximation defined in equation (1), i.e.

$$\mathbf{e}_\sigma \approx \mathbf{e}_\sigma^* = \boldsymbol{\sigma}^* - \boldsymbol{\sigma}_h \tag{5}$$

In the above, the value $\boldsymbol{\sigma}^*$ is a recovered value of $\boldsymbol{\sigma}_h$ which is interpolated from its nodal values by the same basis functions $\mathbf{N}$ as those used for the variable $\mathbf{u}_h$.

The approximation of the error in the energy norm is thus

$$\| \bar{\mathbf{e}} \| = \left(\int_\Omega \mathbf{e}_\sigma^{*\mathrm{T}} \mathbf{D}^{-1} \mathbf{e}_\sigma^* \, d\Omega \right)^{1/2} \tag{6}$$

and this is known as the error estimator. The quality of the error estimator $\| \bar{\mathbf{e}} \|$ is measured by its effectivity index giving the ratio of the estimated to actual errors, i.e.

$$\theta = \frac{\| \bar{\mathbf{e}} \|}{\| \mathbf{e} \|} \tag{7}$$

The error estimator is said to be asymptotically exact if θ approaches unity as the exact error $\| \mathbf{e} \|$ tends to zero (or as $h \to 0$, or as $p \to \infty$). This means that the error estimator will always converge to the exact error while this decreases. Obviously, the reliability of $\| \bar{\mathbf{e}} \|$ is dependent on the quality of σ^*. The following theorem demonstrates how an asymptotically exact error estimator can be achieved.

Theorem 1

Suppose that $\| \mathbf{e}^* \| = \| \mathbf{u} - \mathbf{u}^* \|$ is some error norm of the recovered solution, then the error estimator $\| \bar{\mathbf{e}} \|$ is asymptotically exact if

$$\frac{\| \mathbf{e}^* \|}{\| \mathbf{e} \|} \to 0 \tag{8}$$

as $\| \mathbf{e} \| \to 0$.

Proof. The proof of the theorem is straightforward. We rewrite the error estimator $\| \bar{\mathbf{e}} \|$ as

$$\| \bar{\mathbf{e}} \| = \| \mathbf{u}^* - \mathbf{u}_h \| \equiv \| (\mathbf{u} - \mathbf{u}_h) - (\mathbf{u} - \mathbf{u}^*) \| \tag{9}$$

Using the triangular inequality, we have

$$\| \mathbf{u} - \mathbf{u}_h \| - \| \mathbf{u} - \mathbf{u}^* \| \leqslant \| \bar{\mathbf{e}} \| \leqslant \| \mathbf{u} - \mathbf{u}_h \| + \| \mathbf{u} - \mathbf{u}^* \| \tag{10}$$

or

$$\| \mathbf{e} \| - \| \mathbf{e}^* \| \leqslant \| \bar{\mathbf{e}} \| \leqslant \| \mathbf{e} \| + \| \mathbf{e}^* \| \tag{11}$$

This can alternatively be written, noting the definition of the effectivity index in equation (7), as

$$\left(1 - \frac{\| \mathbf{e}^* \|}{\| \mathbf{e} \|} \right) \leqslant \theta \leqslant \left(1 + \frac{\| \mathbf{e}^* \|}{\| \mathbf{e} \|} \right) \tag{12}$$

The above shows that the effectivity index θ approaches unity as the ratio $\| \mathbf{e}^* \| / \| \mathbf{e} \|$ tends to zero. ∎

The condition that $\| \mathbf{e}^* \| / \| \mathbf{e} \|$ tends to zero as $\| \mathbf{e} \|$ tends to zero in Theorem 1 is achieved if $\| \mathbf{e}^* \|$ converges at a higher rate than $\| \mathbf{e} \|$. It follows that if $\| \mathbf{e}^* \|$ is superconvergent then asymptotic exactness of the error estimator is assured.

Indeed, if we assume that the true error of the finite element approximation converges as

$$\| \mathbf{e} \| = O(h^p) \tag{13a}$$

and the error of the recovered solution as, where $\alpha > 0$

$$\| \mathbf{e}^* \| = O(h^{p+\alpha}) \tag{13b}$$

then a direct corollary of Theorem 1 is that we can write

$$1 - O(h^\alpha) \leqslant \theta \leqslant 1 + O(h^\alpha) \tag{14}$$

With the superconvergent recovery procedure presented in Part 1 of the paper, we have shown that for all examples we have at least

$$\alpha \geqslant 0{\cdot}5 \tag{15}$$

and in fact for many types of elements that $\alpha \geqslant 1$.

We will expect, and indeed will demonstrate in numerical examples, a rapid convergence of the effectivity index to unity.

While a high rate of convergence of $\| e^* \|$ is desirable the error estimator will always be practically applicable providing recovered values are more accurate (though not necessarily superconvergent) than those obtained in the finite element computations. If for instance consistently we have

$$\frac{\| e^* \|}{\| e \|} \equiv \varepsilon \leqslant 0{\cdot}2 \tag{16}$$

the effectivity index of the error estimator will be within practical limits of $0{\cdot}8 \sim 1{\cdot}2$ by equation (12).

The above bounds for the effectivity index apply for the error in the energy norm, however equations (12) and (14) are valid for other norms. We shall, in later sections, demonstrate both the convergence of the energy norm error estimator and the convergence of the pointwise error estimator.

3. NUMERICAL STUDIES

In the following sections we present numerical evidence to demonstrate the convergence of the Z^2 error estimator in which the superconvergent recovered solution is used. In Section 3.1, the convergence of the error estimator in the energy norm is presented. In Section 3.2, the performance of the pointwise error estimator is illustrated. Finally in Section 3.3, we demonstrate the convergence of the error estimator in the adaptive analysis procedure.

In order to compare the performance of the error estimator using different recovery solutions we shall use in the examples the following notation:

N—number of elements

θ^*—effectivity index of the error estimator using the superconvergent recovery procedure of Reference 1

θ^L—effectivity index of the error estimator using global L_2 projection for the recovered solution

θ^{HC}—effectivity index of the error estimator using the Hinton–Campbell[17] local extrapolation for the recovered solution

(for generality we shall sometimes use superscript R with *, L or HC implied)

η—exact relative error in the energy norm

As stated in the previous section, the effectivity index defines how well the error estimator can perform. If the error estimator is asymptotically exact then we expect to find that the estimated errors tend to the exact values as the mesh is refined. However, we also hope that the effectivity index will be close to one, even for coarse meshes, so that adaptive refinement can be performed efficiently.

3.1. Convergence of the energy norm error estimator

We shall in the following examine the convergence of the error estimator in the energy norm with various recovery procedures.

3.1.1. Convergence of the global error estimator

Example 1. We first consider the one dimensional two-point boundary value problem already discussed in the first part of the paper

$$-\frac{\mathrm{d}}{\mathrm{d}x}\left(\frac{\mathrm{d}u}{\mathrm{d}x}\right) + u = f \quad \text{on } I = (0, 1) \tag{17}$$

with boundary conditions

$$u(0) = 0 \quad \text{and} \quad u(1) = 0 \tag{18}$$

The function f is chosen so that the exact solution is of the form

$$u = x^2 - \frac{\mathrm{sh}\,4x}{\mathrm{sh}\,4} \tag{19}$$

where sh is the hyperbolic sine function.
If we define the gradient (or stress) as

$$\sigma = \frac{\mathrm{d}u}{\mathrm{d}x} \tag{20}$$

the error in the energy norm can be written as

$$\|e\| = \left\{ \int_I ((\sigma - \sigma_h)^2 - (u - u_h)^2)\mathrm{d}x \right\}^{1/2} \tag{21}$$

Considering that the error of u_h is of higher order, the error estimator is defined as

$$\|\bar{e}\|^{\mathrm{R}} = \left\{ \sum_{e=1}^{N} (\|\bar{e}\|_e^{\mathrm{R}})^2 \right\}^{1/2} \tag{22}$$

where $\|\bar{e}\|_e^{\mathrm{R}}$ is an element error estimate given as

$$\|\bar{e}\|_e^{\mathrm{R}} = \left\{ \int_{I_e} (\sigma^{\mathrm{R}} - \sigma_h)^2\,\mathrm{d}x \right\}^{1/2} \tag{23}$$

where superscript R represents the type of recovery procedure used.

The problem is solved on a sequence of uniform meshes using linear, quadratic and cubic elements. The convergence of global effectivity indices θ^* and θ^{L} is plotted in Figures 1(a), 1(b) and 1(c) for linear, quadratic and cubic elements respectively. It is observed that θ^* converges to one rapidly for all the elements tested while the mesh is refined. θ^{L} only converges to one at a similar rate to θ^* for linear elements. For quadratic elements, θ^{L} diverges from 1. For cubic elements, θ^{L} again converges to one but at a very slow rate.

The numerical results confirm Theorem 1, i.e. that the effectivity index converges to unity and the error estimate converges to the exact error, if the recovered solution is superconvergent.

The numerical results also demonstrate that to achieve an asymptotically exact *a posteriori* error estimator in the energy norm, the recovered derivatives need not necessarily be super-convergent at every point. We have shown, for instance, in Part 1 that global L_2 projection does
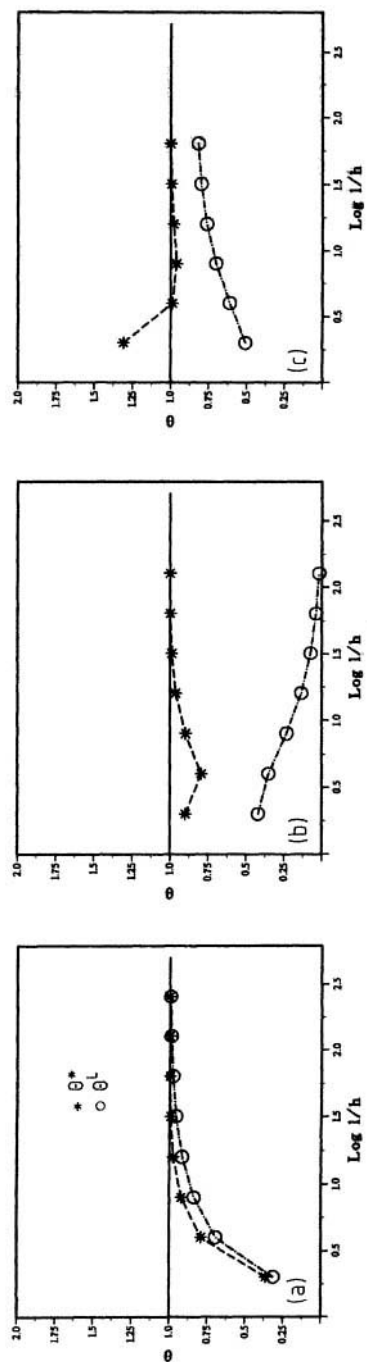
Figure 1. The convergence of global effectivity indices θ^* and θ^L for the one dimensional problem of Example 1: (a) linear element; (b) quadratic element; (c) cubic element

not produce superconvergent values at a boundary for linear elements and yet leads there to convergent estimates.

Example 2. Now consider the following two dimensional problem,

$$- \Delta u = f \quad \text{in } \Omega \tag{24}$$

with boundary condition

$$u = \bar{u} \quad \text{on } \partial \Omega \tag{25}$$

where Ω is a unit square domain $\Omega = (0, 1) \times (0, 1)$ and f is constructed to correspond to the exact solution

$$u(x, y) = (x^3 + y^2) \sin(xy) \tag{26}$$

We define the gradients as

$$\boldsymbol{\sigma} = \nabla u \tag{27}$$

The error in the energy norm is now written as

$$\| e \| = \left\{ \int_{\Omega} (\boldsymbol{\sigma} - \boldsymbol{\sigma}_h)^{\mathrm{T}} (\boldsymbol{\sigma} - \boldsymbol{\sigma}_h) \, d\Omega \right\}^{1/2} \tag{28}$$

and the error estimator is

$$\| \bar{e} \|^{\mathrm{R}} = \left\{ \sum_{e=1}^{N} (\| \bar{e} \|_e^{\mathrm{R}})^2 \right\}^{1/2} \tag{29}$$

with the element error estimate given as

$$\| e \|_e^{\mathrm{R}} = \left\{ \int_{\Omega_e} (\boldsymbol{\sigma}^{\mathrm{R}} - \boldsymbol{\sigma}_h)^{\mathrm{T}} (\boldsymbol{\sigma}^{\mathrm{R}} - \boldsymbol{\sigma}_h) \, d\Omega \right\}^{1/2} \tag{30}$$

Here again superscript R represents the recovery procedure and will be replaced appropriately by L, HC and *.

The problem is solved by various quadrilateral elements (4 node linear, 8 and 9 node quadratic, 12 and 16 node cubic elements) and various triangular elements (3 node linear and 6 node quadratic elements) on sequentially refined uniform meshes.

The numerical results of the performance of the error estimators are plotted in Figures 2(a) to 2(f). It is found, just as for the one dimensional problem, that θ^* converges to one for all the elements tested and in fact θ^* is close to one, even for very coarse meshes. We also observe, from Figures 2(a) and 2(e), that θ^{L} converges to one for linear quadrilateral and triangular elements. In the case of quadratic elements, however, θ^{L} diverges from one for the 9 node quadrilateral element (Figure 2(c)), and is close to 0·5 for the 6 node triangular element (Figure 2(f)). The convergence of θ^{HC} is shown in Figures 2(b) and 2(c) for 8 and 9 node quadrilateral elements. It is noted that θ^{HC} has nearly constant values close to 0·75 for all mesh refinements.

The performance of the error estimator for arbitrarily generated irregular meshes shown in Figure 3 is now considered for various elements. The meshes shown in Figure 3(a) are used for linear and quadratic quadrilateral elements. The mesh shown in Figure 3(b) is used for cubic quadrilateral elements and the meshes shown in Figure 3(c) are used for triangular linear and quadratic elements. Only the numerical results of θ^* are reported and presented in Table I. The numerical results of θ^{L} and θ^{HC} are similar to those for uniform meshes and therefore are not included. It is observed that θ^* is again very close to unity for all the tested elements. This shows
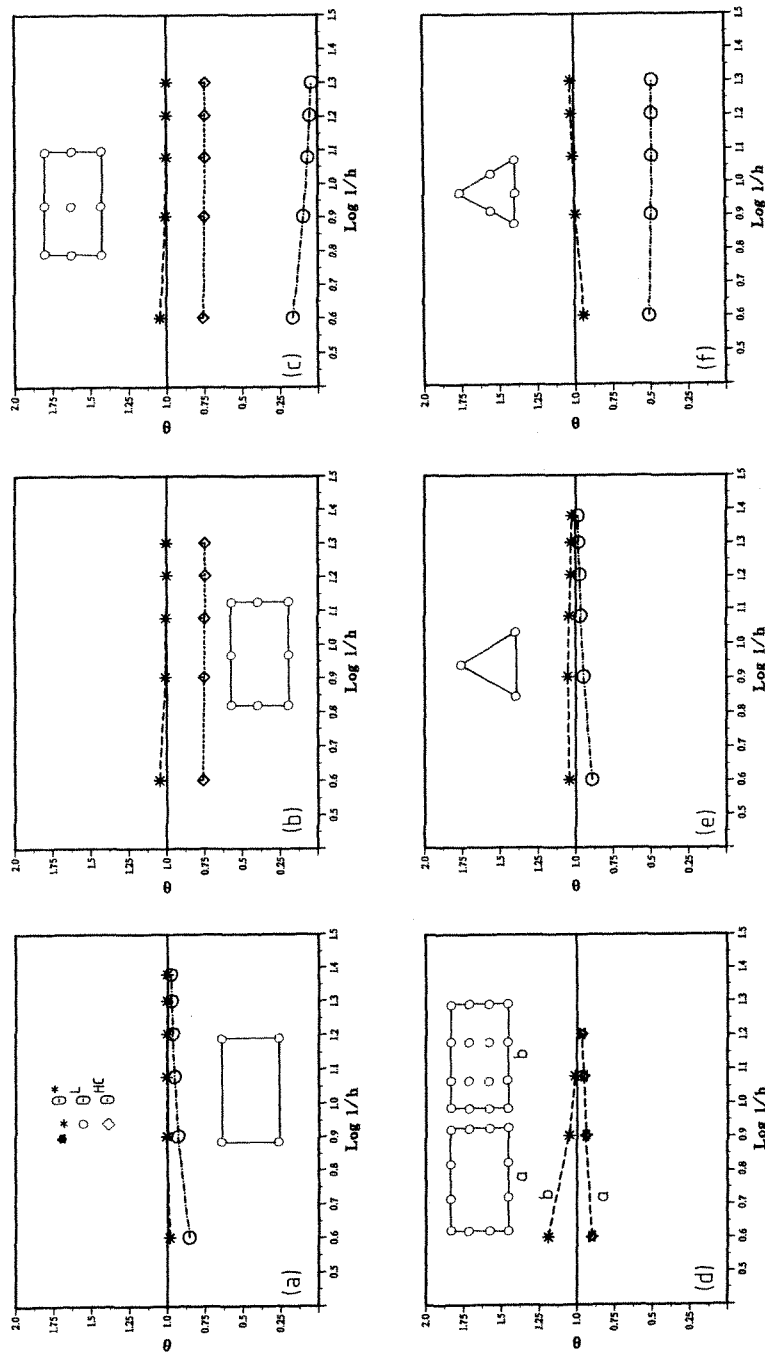
Figure 2. Convergence of the effectivity index for the two dimensional Example 2: (a) 4 node quadrilateral element; (b) 8 node quadrilateral element; (c) 9 node quadrilateral element; (d) 12 and 16 node quadrilateral elements; (e) 3 node triangular element; (f) 6 node triangular element
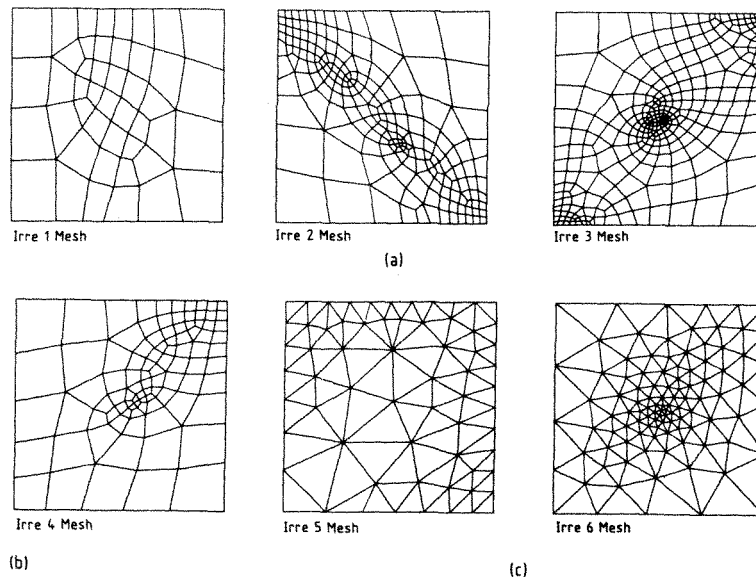
Figure 3. Irregular meshes for Example 2: (a) Three meshes used for linear and quadratic quadrilaterals; (b) mesh used for cubic quadrilaterals; (c) meshes used for linear and quadratic triangles

Table I. The effectivity index θ^* on irregular meshes for various elements. Example 2 (Figure 3)

Mesh	Elements						
	4 node	8 node	9 node	12 node	16 node	3 node	6 node
irr1	0·986	1·005	1·054				
irr2	0·943	1·024	1·038				
irr3	1·022	0·998	1·023				
irr4				0·876	1·019		
irr5						1·073	1·007
irr6						1·112	1·039

that the error estimator $\| \bar{e} \|^*$ will provide reliable error estimation not only for uniform meshes but also for arbitrary irregular meshes—a feature of importance in adaptive analysis procedures.

Example 3. Here we consider a problem of elasticity to demonstrate the convergence of the error estimator in this slightly more complex situation. The problem is the analysis of a portion of an infinite plate with a central circular hole subjected to a unidirectional tensile load. This problem has been considered in the first part of the paper[1] for examining the convergence of the recovered stresses. The geometry of the problem is shown in Figure 4(a). Plane strain conditions are assumed with a Poisson's ratio of 0·3 and Young's modulus $E = 1000$. The plate is loaded on the edges AB and CB by tractions given by an analytic solution in the form of

$$\sigma_x = 1 - \frac{a^2}{r^2} \left(\frac{3}{2} \cos 2\phi + \cos 4\phi \right) + \frac{3}{2} \frac{a^4}{r^4} \cos 4\phi$$
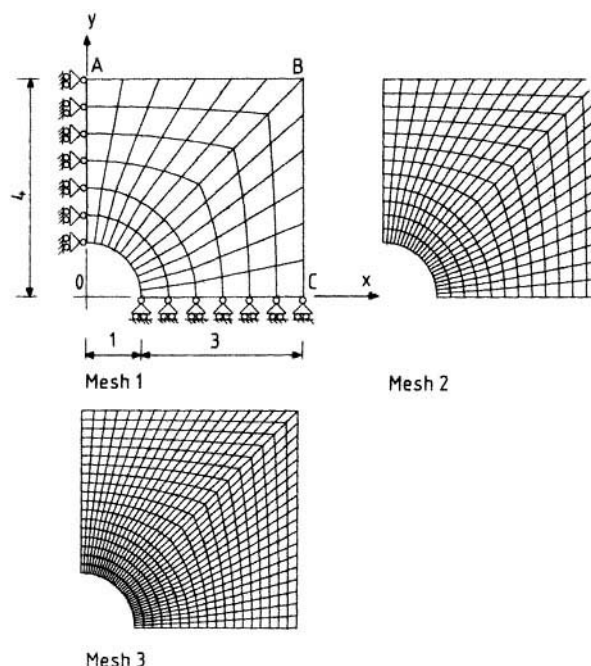
Figure 4. A portion of an infinite plate for uniform tension with a circular hole. Elastic problem of Example 3. Meshes used in the analysis to demonstrate the convergence of error estimator

Table II. The convergence of effectivity indices for the elastic problem of Example 3 (Figure 4)

Mesh	$\theta*$	θ^{HC}	θ^{L}	$\eta(\%)$
1	0·868	1·038	0·396	1·975
2	0·918	1·033	0·328	0·619
3	0·921	0·999	0·268	0·298

$$\sigma_y = -\frac{a^2}{r^2}\left(\frac{1}{2}\cos 2\phi - \cos 4\phi\right) - \frac{3}{2}\frac{a^4}{r^4}\cos 4\phi$$

$$\tau_{xy} = -\frac{a^2}{r^2}\left(\frac{1}{2}\sin 2\phi + \sin 4\phi\right) + \frac{3}{2}\frac{a^4}{r^4}\sin 4\phi \qquad (31)$$

where (r, ϕ) are the usual polar co-ordinates and $a = 1$.

The exact error in the energy norm for the elastic problem is given by equation (4) and the error estimator is written as equation (6) where superscript * may also be replaced by HC or L for appropriate recovery procedures. The performance of the error estimator using different recovery procedures for the recovered solution on various type of elements is similar to that of Example 2. Here only the results for the 9 node element are reported.

Three meshes are used in the analysis and shown in Figure 4. The convergence of the error estimator is presented in Table II. It is observed, from Table II, that $\theta*$ converges to unity (though

does not quite reach it), that θ^{HC} also converges to one and in this case gives values which are better than that of θ^*, and that θ^L is again decreasing for the quadratic element but seems to perform better than in Example 2.

The global effectivity index represents the performance of the global error estimator. It is, however, desirable that the error estimator should provide not only reliable global error estimation but also reliable element error estimation, which is particularly important for mesh refinement in the adaptive analysis. This matter is studied in the next section.

3.1.2. Convergence of the local (element) error estimator. In order to examine the local performance of the element error estimator, we define element effectivity indices as

$$\theta_e^R = \frac{\|\bar{\mathbf{e}}\|_e^R}{\|\mathbf{e}\|_e} \qquad e = 1, 2, \ldots, N \tag{32}$$

and introduce d_e^R as the deviation of the element effectivity indices from unity, i.e.

$$d_e^R = |1 - \theta_e^R| \tag{33}$$

Obviously d_e^R tends to zero while θ_e^R converges to one.

Example 4. We consider again the problem of Example 2 with the 9 node element used in the analysis on a 12×12 uniform subdivision.

The contours of the exact and estimated average element error are illustrated in Plates 1(a), 1(b), 1(c) and 1(d). It is clearly observed, from Plates 1(a) and 1(b), that the distribution of the estimated error $\|\bar{e}\|_e^*$ is almost identical with the distribution of the exact error. The global effectivity index $\theta^* = 1.003$. It is also found that, although the global effectivity index $\theta^{HC} = 0.747$, the distribution of $\|\bar{e}\|_e^{HC}$ is completely different from the distribution of the exact error, and that $\|\bar{e}\|_e^L$ severely underestimated the error with global effectivity index $\theta^L = 0.067$.

The deviations d_e^*, d_e^{HC} and d_e^L of element effectivity indices are presented in Plates 2(a), 2(b) and 2(c) respectively. It is evident that in most elements θ_e^* is close to one (Plate 2(a)). By comparing Plates 1(a), 1(b) and 2(a), we found that, where d_e^* is large, the exact error $\|e\|_e$ is in fact very small and the error estimator has overestimated the error on these elements. It should be noted, from Plates 2(b) and 2(c), that neither $\|\bar{e}\|_i^{HC}$ nor $\|\bar{e}\|_i^L$ provide a reliable local element error estimation.

Example 5. The elastic problem of Example 3 is again considered. The problem is solved on mesh 2 of Figure 4. The computed global effectivity indices are shown in Table II with $\theta^* = 0.918$, $\theta^{HC} = 1.033$ and $\theta^L = 0.328$.

The contours of the exact and estimated average element error are presented in Plate 3 and the deviations of the effectivity indices are plotted in Plate 4. It is again observed that the distribution of $\|\bar{\mathbf{e}}\|_e^*$ is almost identical with the distribution of the exact error (Plates 3(a) and 3(b)) and that θ_e^* is very close to unity on most of the elements (Plate 4(a)). More significantly, we find that, although the global effectivity index of θ^{HC} is closer to unity than that of θ^*, the deviation of the element effectivity index θ_e^* is much smaller than that of θ_e^{HC} for most of the elements (Plates 4(a) and 4(b)), showing that $\|\bar{\mathbf{e}}\|_e^*$ provides the most reliable element error estimation.

We also observe, by comparing Plates 3(a), 3(c) and 3(d) that, although the deviation of element error estimator is large for θ_e^{HC} and θ_e^L (Plates 4(b) and 4(c)), the corresponding error estimators provide, however, some indication for the exact error distribution.

The numerical experiments presented in this section demonstrate that if a recovered super-convergent solution is used in the energy norm of the Zienkiewicz–Zhu error estimator, the error

estimator is reliable and accurate both globally and locally for each element, as predicted by Theorem 1 of Section 2.

3.2. The performance of pointwise error estimator

The assessment of pointwise accuracy of the finite element approximation is often desirable in practical engineering computations. However, pointwise error estimation is much more difficult than the error estimation in the energy norm. An accurate estimation of the pointwise error has so far been achieved only for one dimensional problems.[13] We shall demonstrate in the following, for a wide range of problems, that an accurate pointwise error estimation can be achieved using the superconvergent recovery procedures discussed in Part 1 of the paper.[1]

Example 6. We consider the problem of Example 2. The pointwise error of the gradients (stresses) is defined as

$$|e_{\bar{\sigma}}| = |\bar{\sigma} - \bar{\sigma}_h| \tag{34}$$

where

$$\bar{\sigma} = \sqrt{\left(\frac{\partial u}{\partial x}\right)^2 + \left(\frac{\partial u}{\partial y}\right)^2} \tag{35}$$

is termed the *effective gradient*.

At an element boundary point, $|e_{\bar{\sigma}}|$ is multivalued owing to the discontinuity of $\bar{\sigma}_h$. The maximum value of $|e_{\bar{\sigma}}|$ at such points is defined as its value in equation (34).

The pointwise error estimator is written as

$$|\bar{e}_{\bar{\sigma}}|^R = |\bar{\sigma}^R - \bar{\sigma}_h| \tag{36}$$

The multivalue situation for $|\bar{e}_{\bar{\sigma}}|^R$ at element boundary nodal points is treated in the same manner as that for $|e_{\bar{\sigma}}|$.

We note that at a particular point of the domain where the problem is defined Theorem 1 is obviously applicable to $|\bar{e}_{\bar{\sigma}}|^R$. The convergence of $|\bar{e}_{\bar{\sigma}}|^R$ is therefore expected if the recovered solution used in the error estimator is pointwise superconvergent.

The effectivity index for the pointwise error estimator is defined as

$$\theta_i^R = \frac{|\bar{e}_{\bar{\sigma}}|^R}{|e_{\bar{\sigma}}|} \tag{37}$$

and the deviation of the effectivity index for the pointwise error estimator is defined as

$$d_i^R = |1 - \theta_i^R| \tag{38}$$

at each point i.

The problem is solved on a 12×12 mesh using 9 node quadrilateral elements. The nodal points are chosen as sampling points in the error estimation.

The contours of the distribution of the exact and estimated pointwise effective gradient error are presented in Plate 5. The deviations of the effectivity indices are illustrated in Plate 6.

It is observed, from Plates 5(a) and 5(b), that the distribution of $|\bar{e}_{\bar{\sigma}}|^*$ is almost identical with the distribution of the exact error. The effectivity index θ^* is close to unity at most points in the domain (Plate 6(a)). Plates 5(c) and 5(d) and Plates 6(b) and 6(c) show that $|\bar{e}_{\bar{\sigma}}|^{HC}$ and $|\bar{e}_{\bar{\sigma}}|^L$ are not useful for use as pointwise error estimators.
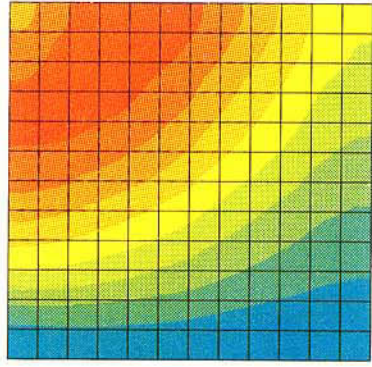
(a) Contour of the distribution of the exact energy norm error
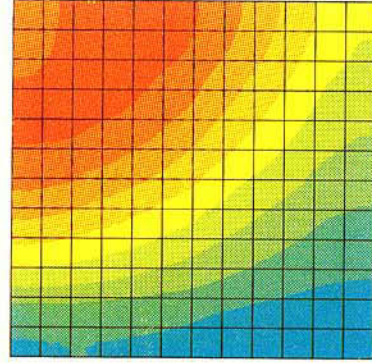
(b) Contour of the distribution of the energy norm error estimator (new recovery)

(d) Contour of the distribution of the energy norm error estimator (L2 projection)

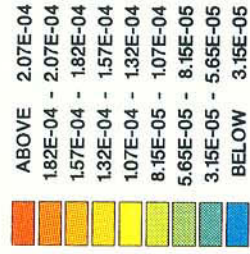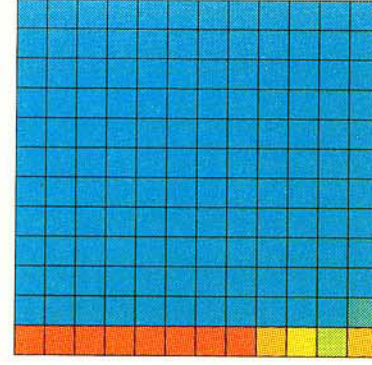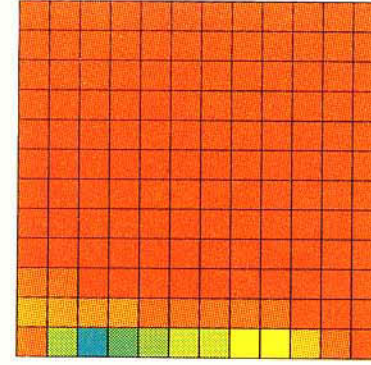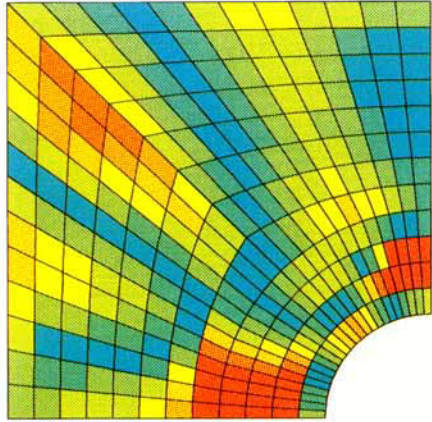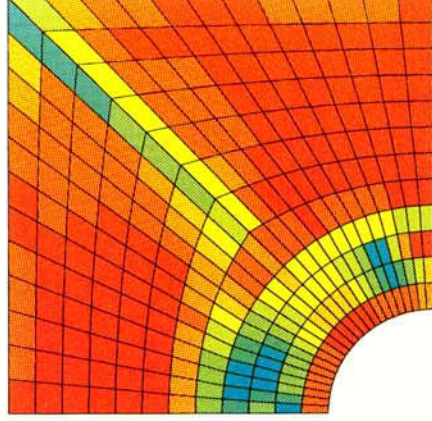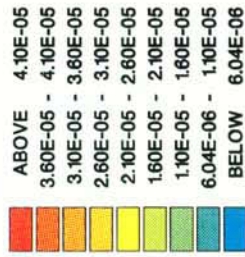(c) Contour of the distribution of the energy norm error estimator (HC smoothing)

ABOVE   2.07E-04
1.82E-04 - 2.07E-04
1.57E-04 - 1.82E-04
1.32E-04 - 1.57E-04
1.07E-04 - 1.32E-04
8.15E-05 - 1.07E-04
5.65E-05 - 8.15E-05
3.15E-05 - 5.65E-05
BELOW   3.15E-05
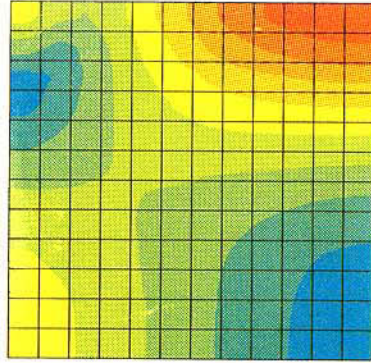
Plate 1. Distribution of the exact and estimated average element energy norm error on 12 x 12 mesh. Example 4

(a) Deviation of element effectivity index for energy norm error estimator (new recovery)
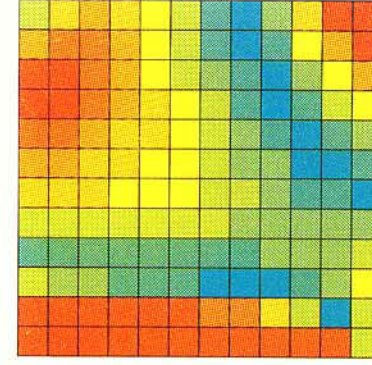
(b) Deviation of element effectivity index for energy norm error estimator (HC smoothing)

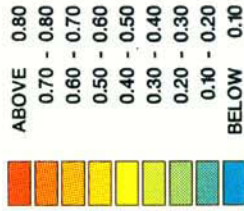(c) Deviation of element effectivity index for energy norm error estimator (L2 projection)

ABOVE   0.80
0.70 - 0.80
0.60 - 0.70
0.50 - 0.60
0.40 - 0.50
0.30 - 0.40
0.20 - 0.30
0.10 - 0.20
BELOW   0.10
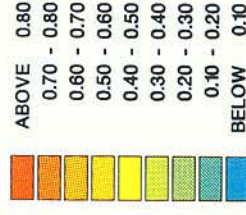
Plate 2. Deviation of the element effectivity index ($|1-\theta^R|$) for error estimator using various recovered solutions shown in Plate 1
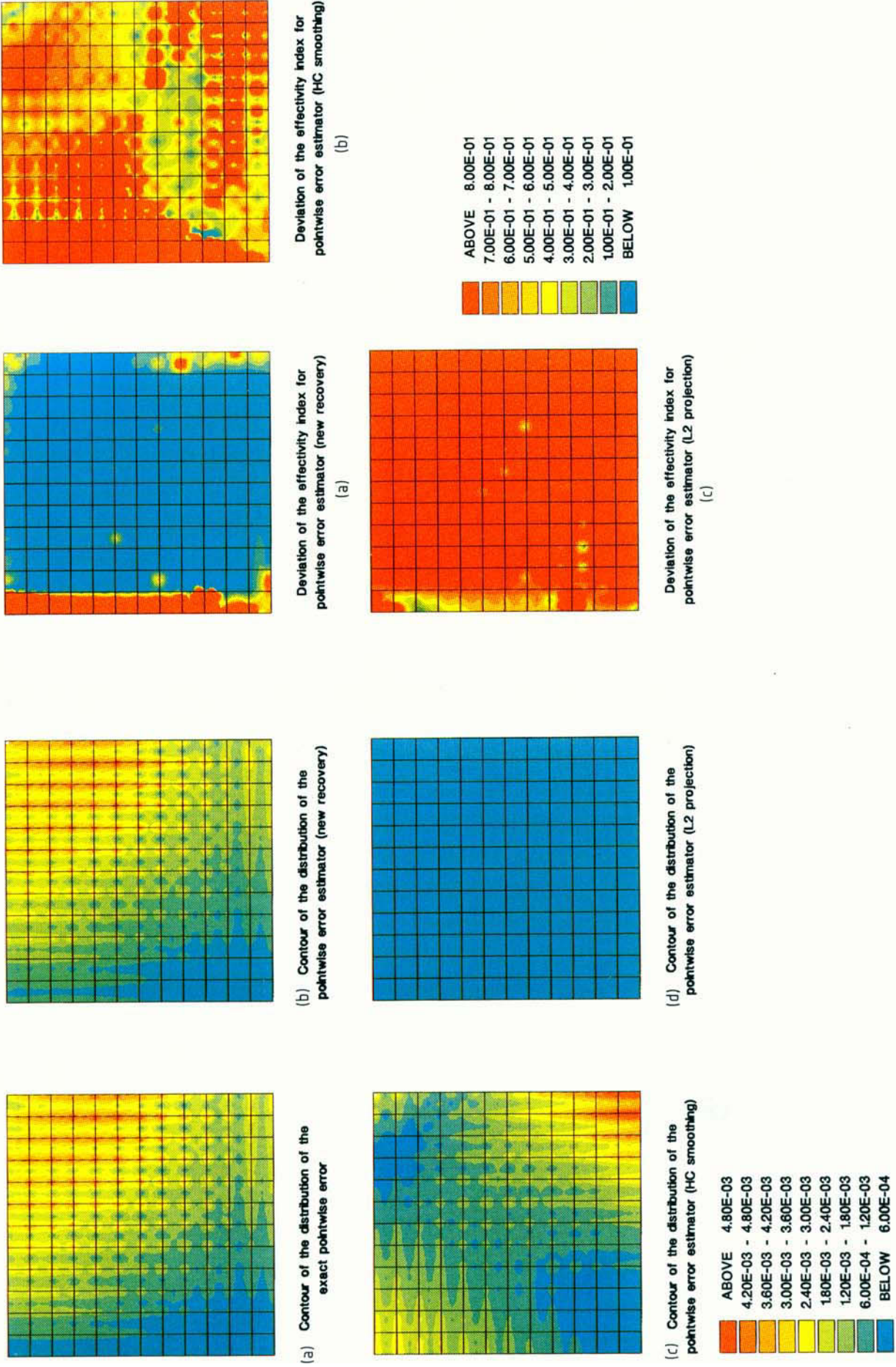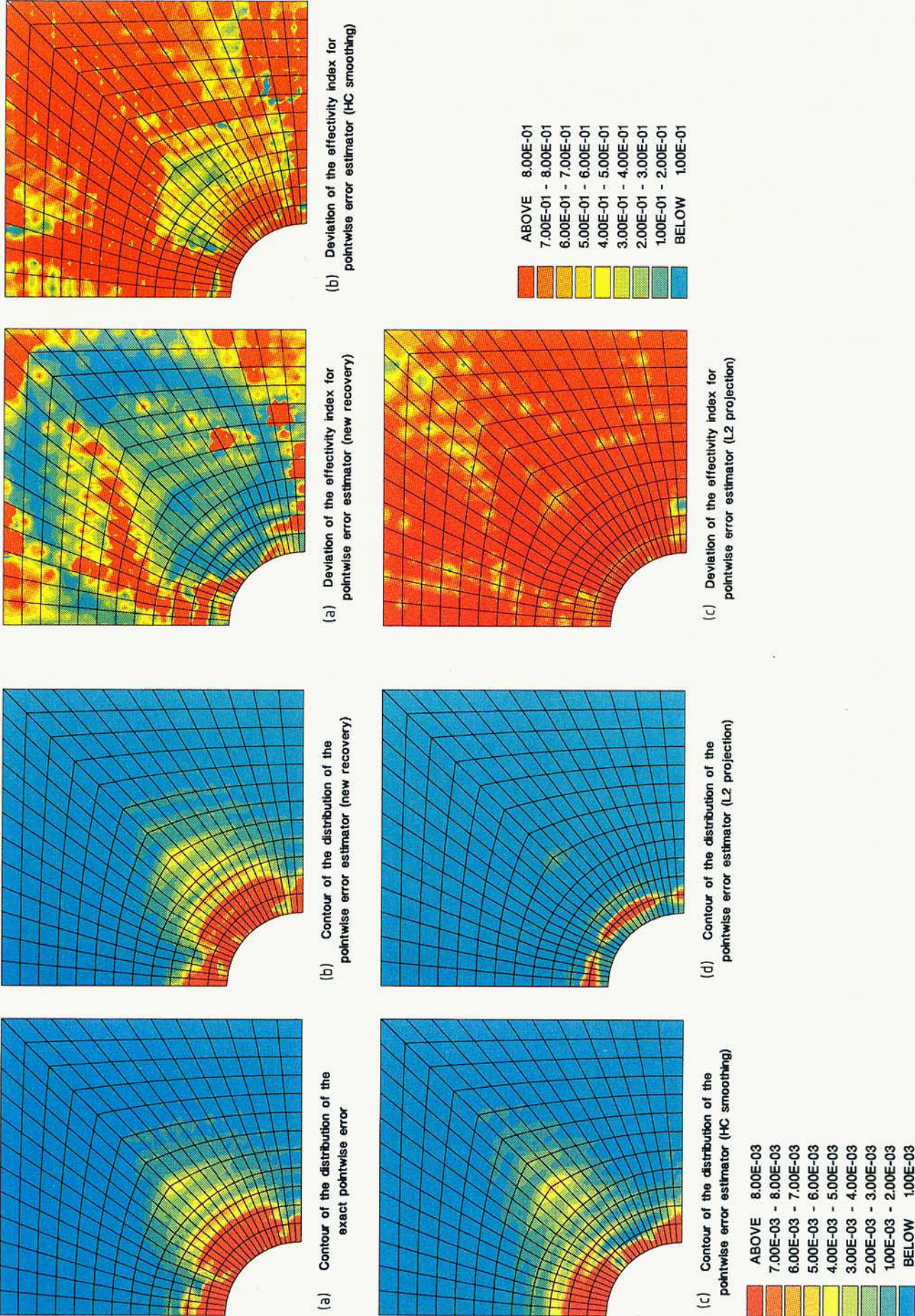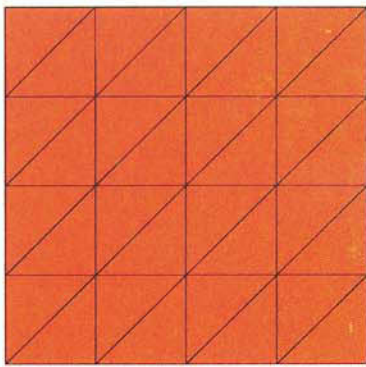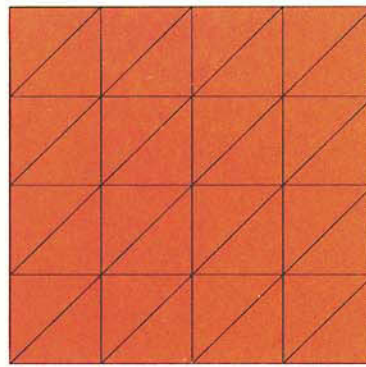
(a) Contour of the distribution of the exact energy norm error

(b) Contour of the distribution of the energy norm error estimator (new recovery)

(c) Contour of the distribution of the energy norm error estimator (HC smoothing)

(d) Contour of the distribution of the energy norm error estimator (L2 projection)

ABOVE   4.10E–05
3.60E–05 – 4.10E–05
3.10E–05 – 3.60E–05
2.60E–05 – 3.10E–05
2.10E–05 – 2.60E–05
1.60E–05 – 2.10E–05
1.10E–05 – 1.60E–05
6.04E–06 – 1.10E–05
BELOW   6.04E–06
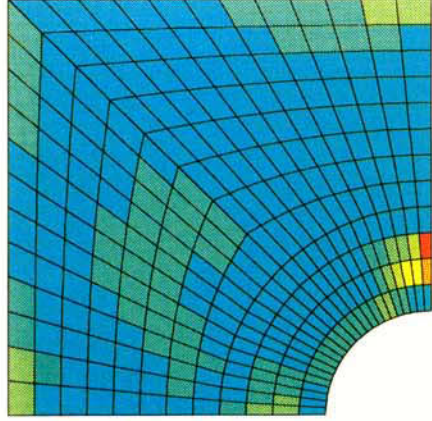
Plate 3. Distribution of the exact and estimated average element energy norm error on mesh 2 of Figure 4. Example 5

(a) Deviation of element effectivity index for energy norm error estimator (new recovery)

(b) Deviation of element effectivity index for energy norm error estimator (HC smoothing)

(c) Deviation of element effectivity index for energy norm error estimator (L2 projection)

ABOVE   0.80
0.70 – 0.80
0.60 – 0.70
0.50 – 0.60
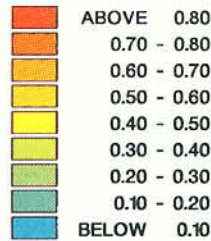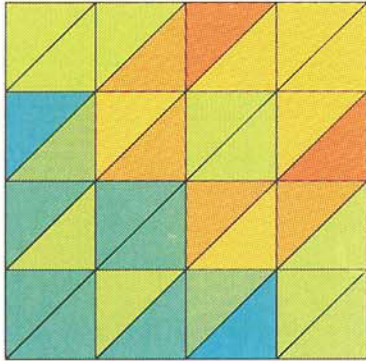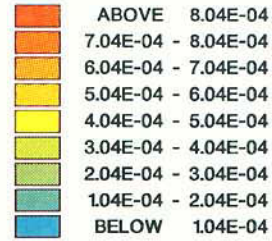0.40 – 0.50
0.30 – 0.40
0.20 – 0.30
0.10 – 0.20
BELOW   0.10

Plate 4. Deviation of the element effectivity index ($|1-\theta^R|$) for error estimator using various recovered solutions shown in Plate 3

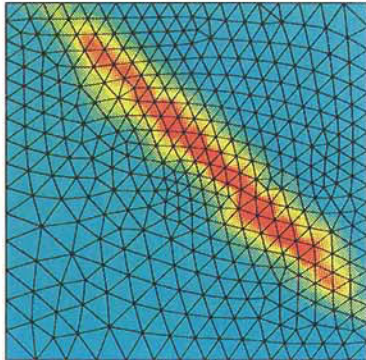(a) Contour of the distribution of the exact pointwise error

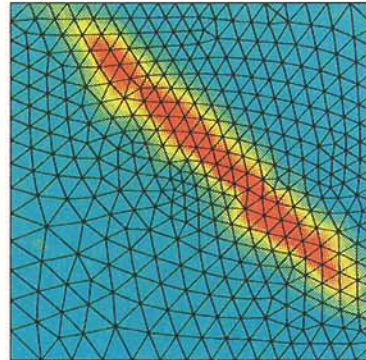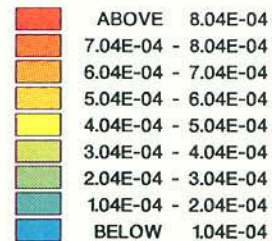(b) Contour of the distribution of the pointwise error estimator (new recovery)

(c) Contour of the distribution of the pointwise error estimator (HC smoothing)

ABOVE	4.80E-03
4.20E-03	-	4.80E-03
3.60E-03	-	4.20E-03
3.00E-03	-	3.60E-03
2.40E-03	-	3.00E-03
1.80E-03	-	2.40E-03
1.20E-03	-	1.80E-03
6.00E-04	-	1.20E-03
BELOW	6.00E-04

Plate 5. Distribution of the exact and estimated pointwise effective gradient error on 12 x 12 mesh. Example 6

Deviation of the effectivity index for pointwise error estimator (new recovery)
(a)

Deviation of the effectivity index for pointwise error estimator (HC smoothing)
(b)

Deviation of the effectivity index for pointwise error estimator (L2 projection)
(c)

(d) Contour of the distribution of the pointwise error estimator (L2 projection)

ABOVE	8.00E-01
7.00E-01	-	8.00E-01
6.00E-01	-	7.00E-01
5.00E-01	-	6.00E-01
4.00E-01	-	5.00E-01
3.00E-01	-	4.00E-01
2.00E-01	-	3.00E-01
1.00E-01	-	2.00E-01
BELOW	1.00E-01

Plate 6. Deviation of pointwise effectivity index ($|1-\theta^R|$) for error estimator using various recovered solutions shown in Plate 5

(a) Contour of the distribution of the exact pointwise error

(b) Contour of the distribution of the pointwise error estimator (new recovery)

(c) Contour of the distribution of the pointwise error estimator (HC smoothing)

(d) Contour of the distribution of the pointwise error estimator (L2 projection)

ABOVE   8.00E-03
7.00E-03 - 8.00E-03
6.00E-03 - 7.00E-03
5.00E-03 - 6.00E-03
4.00E-03 - 5.00E-03
3.00E-03 - 4.00E-03
2.00E-03 - 3.00E-03
1.00E-03 - 2.00E-03
BELOW   1.00E-03

Plate 7. Distribution of the exact and estimated pointwise effective stress error on mesh 2 of Figure 4. Example 7

(a) Deviation of the effectivity index for pointwise error estimator (new recovery)

(b) Deviation of the effectivity index for pointwise error estimator (HC smoothing)

(c) Deviation of the effectivity index for pointwise error estimator (L2 projection)

ABOVE   8.00E-01
7.00E-01 - 8.00E-01
6.00E-01 - 7.00E-01
5.00E-01 - 6.00E-01
4.00E-01 - 5.00E-01
3.00E-01 - 4.00E-01
2.00E-01 - 3.00E-01
1.00E-01 - 2.00E-01
BELOW   1.00E-01

Plate 8. Deviation of pointwise effectivity index ($|1-\theta^R|$) for error estimator using various recovered solutions as shown in Plate 7

(a) Contour of the distribution of the exact energy norm error

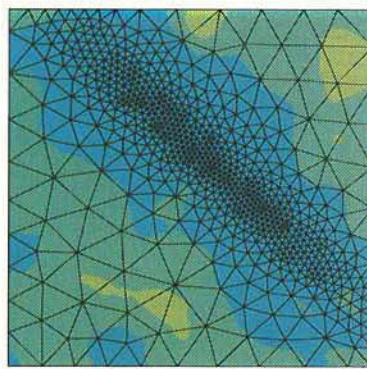(b) Contour of the distribution of the energy norm error estimator (new recovery)

	ABOVE 8.04E-04
	7.04E-04 - 8.04E-04
	6.04E-04 - 7.04E-04
	5.04E-04 - 6.04E-04
	4.04E-04 - 5.04E-04
	3.04E-04 - 4.04E-04
	2.04E-04 - 3.04E-04
	1.04E-04 - 2.04E-04
	BELOW 1.04E-04

	ABOVE 0.80
	0.70 - 0.80
	0.60 - 0.70
	0.50 - 0.60
	0.40 - 0.50
	0.30 - 0.40
	0.20 - 0.30
	0.10 - 0.20
	BELOW 0.10

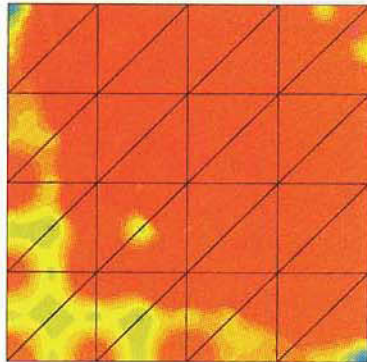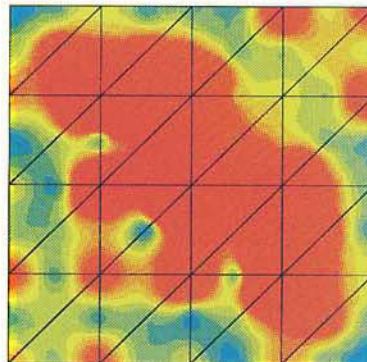(c) Deviation of element effectivity index for energy norm error estimator (new recovery)
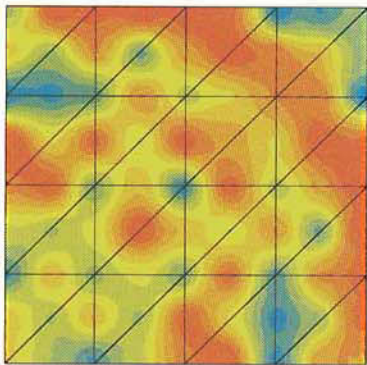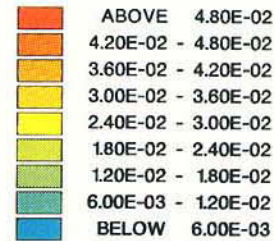
Plate 9. Exact and estimated average element energy norm error and deviation of element effectivity index ($|1-\theta^*|$) for mesh 1 of Figure 9. Example 8

(a) Contour of the distribution of the exact energy norm error

(b) Contour of the distribution of the energy norm error estimator (new recovery)

	ABOVE 8.04E-04
	7.04E-04 - 8.04E-04
	6.04E-04 - 7.04E-04
	5.04E-04 - 6.04E-04
	4.04E-04 - 5.04E-04
	3.04E-04 - 4.04E-04
	2.04E-04 - 3.04E-04
	1.04E-04 - 2.04E-04
	BELOW 1.04E-04

	ABOVE 0.80
	0.70 - 0.80
	0.60 - 0.70
	0.50 - 0.60
	0.40 - 0.50
	0.30 - 0.40
	0.20 - 0.30
	0.10 - 0.20
	BELOW 0.10
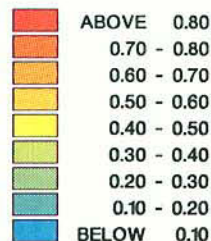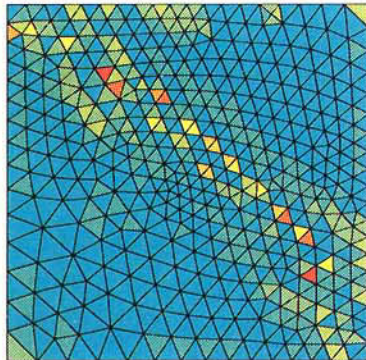
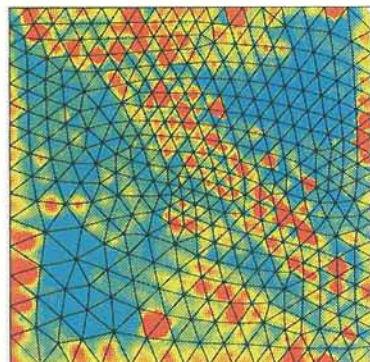(c) Deviation of element effectivity index for energy norm error estimator (new recovery)

Plate 10. Exact and estimated average element energy norm error and deviation of element effectivity index ($|1-\theta^*|$) for mesh 2 of Figure 9. Example 8

(a) Contour of the distribution of the
exact energy norm error

(b) Contour of the distribution of the
energy norm error estimator (new recovery)

	ABOVE 8.04E-04
	7.04E-04 - 8.04E-04
	6.04E-04 - 7.04E-04
	5.04E-04 - 6.04E-04
	4.04E-04 - 5.04E-04
	3.04E-04 - 4.04E-04
	2.04E-04 - 3.04E-04
	1.04E-04 - 2.04E-04
	BELOW 1.04E-04

	ABOVE 0.80
	0.70 - 0.80
	0.60 - 0.70
	0.50 - 0.60
	0.40 - 0.50
	0.30 - 0.40
	0.20 - 0.30
	0.10 - 0.20
	BELOW 0.10
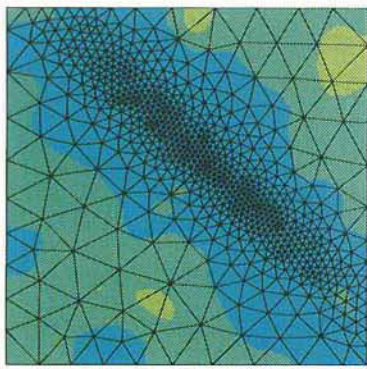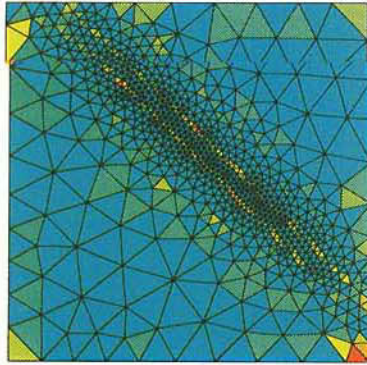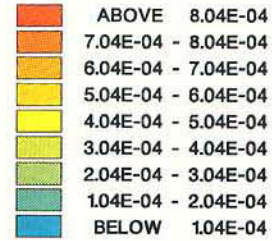
c) Deviation of element effectivity index for
energy norm error estimator (new recovery)
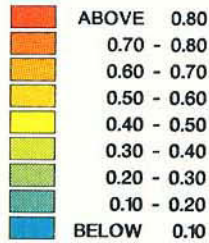
Plate 11. Exact and estimated average element
energy norm error and deviation of element
effectivity index ($|1-\theta^*|$) for mesh 3 of Figure 9.
Example 8

(a) Contour of the distribution of the
exact pointwise error

(b) Contour of the distribution of the
pointwise error estimator (new recovery)

	ABOVE 4.80E-02
	4.20E-02 - 4.80E-02
	3.60E-02 - 4.20E-02
	3.00E-02 - 3.60E-02
	2.40E-02 - 3.00E-02
	1.80E-02 - 2.40E-02
	1.20E-02 - 1.80E-02
	6.00E-03 - 1.20E-02
	BELOW 6.00E-03

	ABOVE 8.00E-01
	7.00E-01 - 8.00E-01
	6.00E-01 - 7.00E-01
	5.00E-01 - 6.00E-01
	4.00E-01 - 5.00E-01
	3.00E-01 - 4.00E-01
	2.00E-01 - 3.00E-01
	1.00E-01 - 2.00E-01
	BELOW 1.00E-01

c) Deviation of the effectivity index for
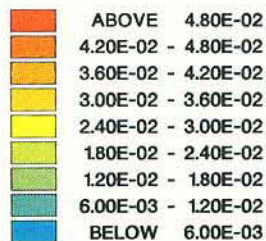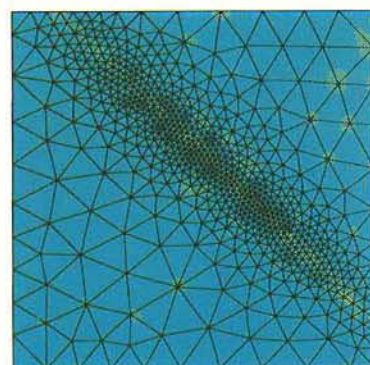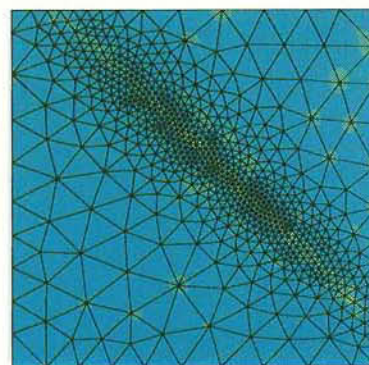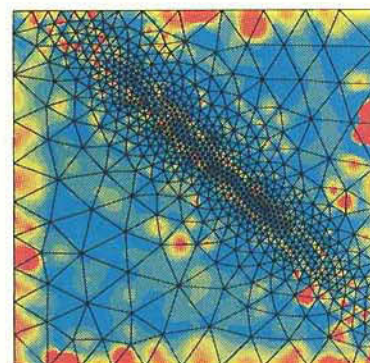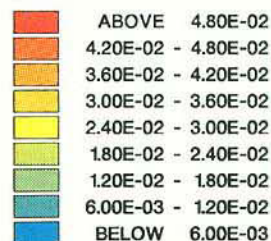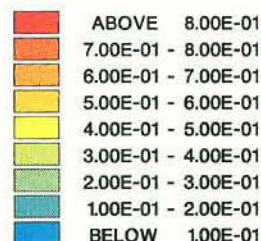pointwise error estimator (new recovery)
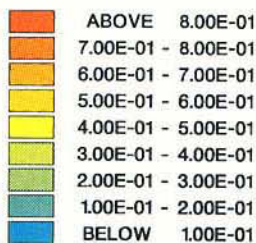
Plate 12. Exact and estimated pointwise effective
gradient error and deviation of pointwise effectivity
index ($|1-\theta^*|$) for mesh 1 of Figure 9. Example 8

(a) Contour of the distribution of the
exact pointwise error

(b) Contour of the distribution of the
pointwise error estimator (new recovery)

	ABOVE 4.80E-02
	4.20E-02 - 4.80E-02
	3.60E-02 - 4.20E-02
	3.00E-02 - 3.60E-02
	2.40E-02 - 3.00E-02
	1.80E-02 - 2.40E-02
	1.20E-02 - 1.80E-02
	6.00E-03 - 1.20E-02
	BELOW 6.00E-03

	ABOVE 8.00E-01
	7.00E-01 - 8.00E-01
	6.00E-01 - 7.00E-01
	5.00E-01 - 6.00E-01
	4.00E-01 - 5.00E-01
	3.00E-01 - 4.00E-01
	2.00E-01 - 3.00E-01
	1.00E-01 - 2.00E-01
	BELOW 1.00E-01
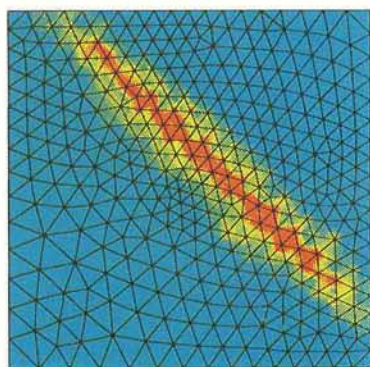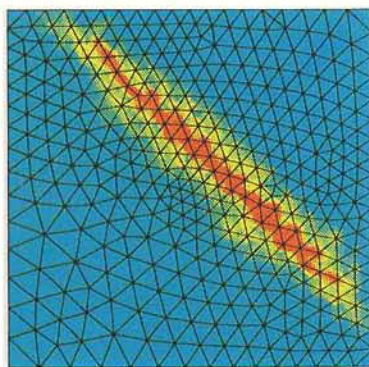
(c) Deviation of the effectivity index for
pointwise error estimator (new recovery)
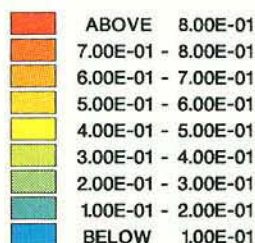
Plate 13. Exact and estimated pointwise effective
gradient error and deviation of pointwise effectivity
index ($|1-\theta^*|$) for mesh 2 of Figure 9. Example 8

(a) Contour of the distribution of the
exact pointwise error

(b) Contour of the distribution of the
pointwise error estimator (new recovery)

	ABOVE 4.80E-02
	4.20E-02 - 4.80E-02
	3.60E-02 - 4.20E-02
	3.00E-02 - 3.60E-02
	2.40E-02 - 3.00E-02
	1.80E-02 - 2.40E-02
	1.20E-02 - 1.80E-02
	6.00E-03 - 1.20E-02
	BELOW 6.00E-03

	ABOVE 8.00E-01
	7.00E-01 - 8.00E-01
	6.00E-01 - 7.00E-01
	5.00E-01 - 6.00E-01
	4.00E-01 - 5.00E-01
	3.00E-01 - 4.00E-01
	2.00E-01 - 3.00E-01
	1.00E-01 - 2.00E-01
	BELOW 1.00E-01

(c) Deviation of the effectivity index for
pointwise error estimator (new recovery)

Plate 14. Exact and estimated pointwise effective
gradient error and deviation of pointwise effectivity
index ($|1-\theta^*|$) for mesh 3 of Figure 9. Example 8

Example 7. Here we consider the elastic problem of Example 3. For the elastic problem we shall consider the pointwise error of effective stress. The error is defined by equation (34) and the error estimator is defined by equation (36). Here, however, the *effective stress* is defined conventionally as

$$\bar{\sigma} = \sqrt{3J'_2} = \sqrt{\tfrac{3}{2}\sigma'_{ij}\sigma'_{ij}} \tag{39}$$

where J'_2 is the second invariant of the deviatoric stress σ'_{ij} and

$$\sigma'_{ij} = \sigma_{ij} - \tfrac{1}{3}\delta_{ij}\sigma_{kk} \quad i,j,k = 1,2,3 \tag{40}$$

where δ_{ij} is the Kronecker delta.

Mesh 2 of Figure 4 is used in the analysis and the nodal points are again used as sampling points for error calculation. The contours of the exact and estimated pointwise error distribution are illustrated in Plate 7 and the deviations of the effectivity indices are plotted in Plate 8.

It is observed, as in Example 6, that the distribution of $|\bar{e}_{\bar{\sigma}}|^*$ (Plate 7(b)) is strikingly similar to that of the exact error (Plate 7(a)). We also found that $|\bar{e}_{\bar{\sigma}}|^{\text{HC}}$ and $|\bar{e}_{\bar{\sigma}}|^{\text{L}}$ (Plates 7(c) and 7(d)) are not suitable for local error estimation although they provide an indication of the distribution of the true error. The observation is confirmed by the deviation of the effectivity indices (Plates 8(a), 8(b) and 8(c)).

It is interesting to note, by observing Plates 5(a), 5(b) and 6(a) and Plates 7(a), 7(b) and 8(a), that the pointwise error estimator $|\bar{e}_{\bar{\sigma}}|^*$ provides a particularly accurate error estimation at the points where the error is large.

We also note, from Plates 5(a) and 7(a), that the true pointwise error is usually larger at corner nodes of the element, are smaller at internal nodes for the 9 node quadrilateral elements used in the analysis.

The accurate estimation of the pointwise error has been achieved by using the recovered superconvergent solution on a particular mesh as shown in this section. We shall report the convergence of the pointwise error estimator through an example of adaptive analysis in the next section.

3.3. The performance of the error estimators in adaptive analysis

We shall in this section present the performance of the error estimator in the context of adaptive analysis. The automatic adaptive mesh refinement process used in the analysis follows the strategies proposed in References 2 and 14, in which details can be found.

Example 8. The governing equation of the problem is

$$-\Delta u = f \quad \text{in } \Omega \tag{41}$$

with boundary condition

$$u = 0 \quad \text{on } \partial\Omega \tag{42}$$

where Ω is a unit square domain $\Omega = (0,1) \times (0,1)$ and f is chosen so that the exact solution is of the form

$$u = x(1-x)y(1-y)\tan^{-1}(\alpha(\xi - \xi_0)) \tag{43}$$

where $\xi = (x+y)/\sqrt{2}$, $\xi_0 = 0.8$ and $\alpha = 20$.

This problem has been considered by Oden *et al.*[8] for testing various error estimators. The solution of the problem exhibits a relatively sharp transition of gradients in some areas. The

contours of the exact solution of $\partial u/\partial x$ and $\partial u/\partial y$ are plotted in Figure 5. The problem is analysed by the adaptive analysis procedure using linear 4 node quadrilateral and 3 node triangular elements and quadratic 9 node quadrilateral and 6 node triangular elements. The prescribed accuracy for linear elements is 10 per cent of the energy norm relative error, and for quadratic elements is 1 per cent of the energy norm relative error.

The automatically generated meshes by the adaptive procedure are presented in Figures 6–9 for 4 node, 3 node, 9 node and 6 node elements respectively. The obtained exact relative error η and

Base contour value = -0.365100
Maximum contour value = 0.852200
Contour interval = 0.060865

Base contour value = -0.365100
Maximum contour value = 0.852200
(b) Contour interval = 0.060865
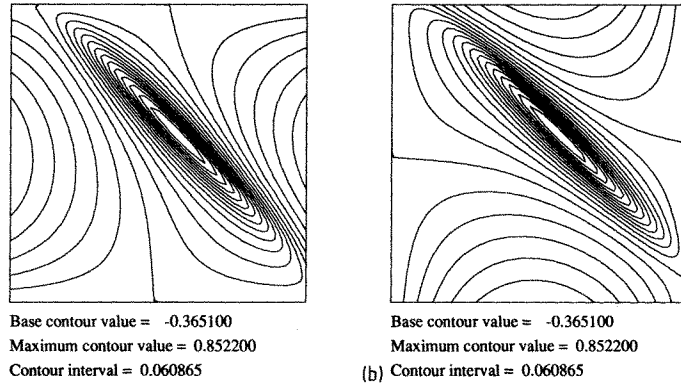
Figure 5. Contour of (a) $\partial u/\partial x$ and (b) $\partial u/\partial y$ for Example 8

Mesh 1   16 elements (9 D.O.F.)
η=57.652% θ^* =1.064
              θ^L = 0.803

Mesh 2   451 elements (414 D.O.F.)
η=13.728% θ^* =1.155
              θ^L = 0.994

Mesh 3   1178 elements (1155 D.O.F.)
η=9.897% θ^* =1.024
              θ^L = 0.941
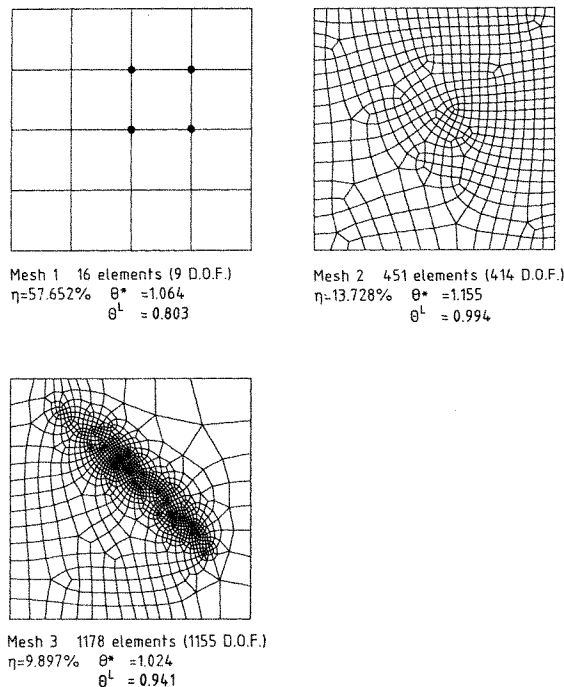
Figure 6. Adaptive analysis of Example 10. Mesh refinement aiming at 10 per cent accuracy. 4 node element
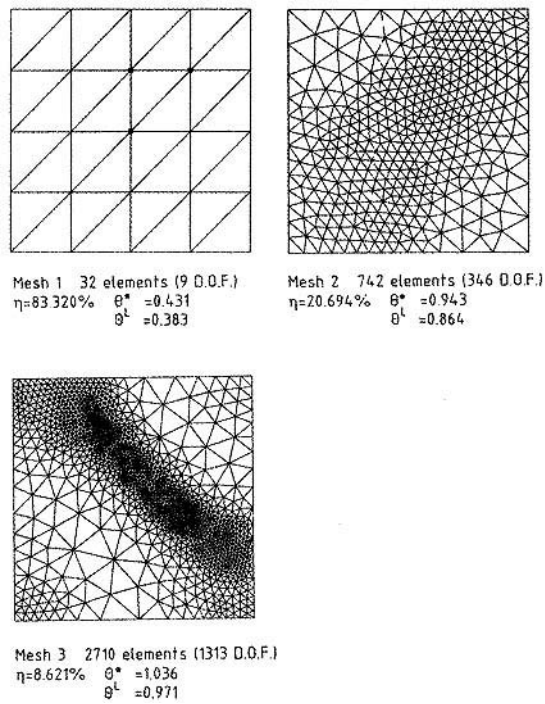
Figure 7. Adaptive analysis of Example 10. Mesh refinement aiming at 10 per cent accuracy. 3 node element
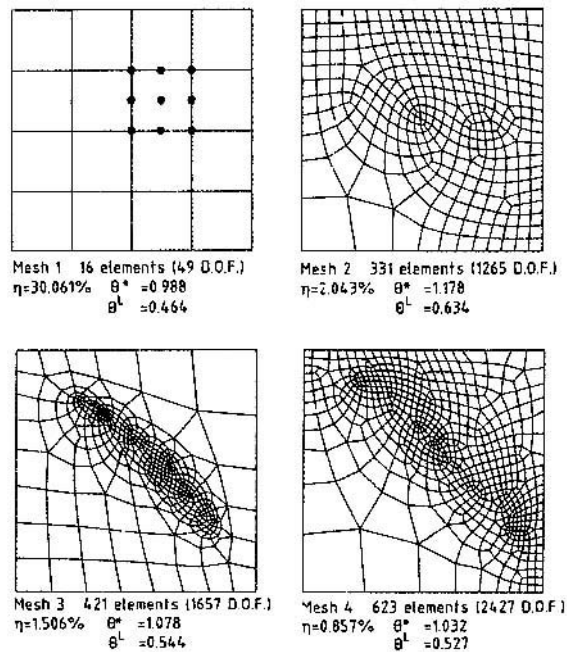
Figure 8. Adaptive analysis of Example 10. Mesh refinement aiming at 1 per cent accuracy. 9 node element

Mesh 1   27 elements (252 D.O.F.)
η=8.258% θ^* =1.110
            θ^L =0.615

Mesh 2   101 elements (876 D.O.F.)
η=3.118% θ^* =1.057
            θ^L =0.518

Mesh 3   229 elements (1940 D.O.F.)
η=0.634 θ^* =1.048
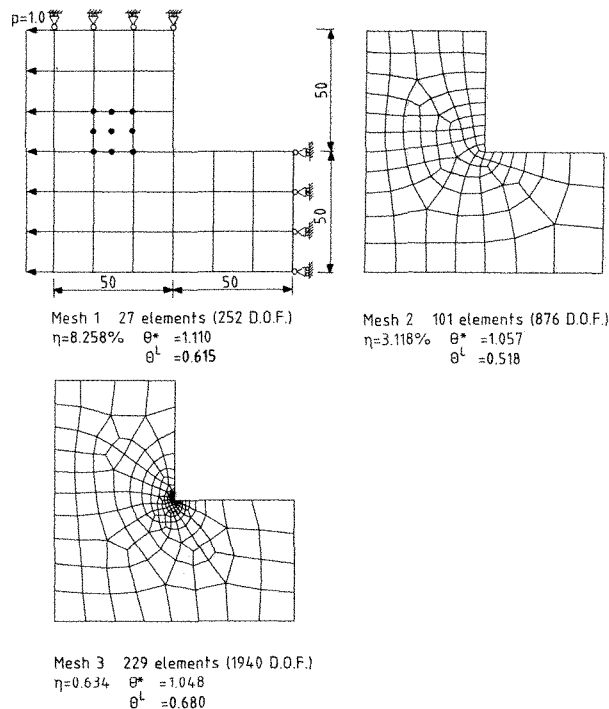 θ^L =0.680

Figure 10. An L-shaped domain in plane stress condition. Adaptive analysis to achieve 1 per cent accuracy. 9 node element. Example 9

zero when uniform mesh refinements are used in the computations. However, when adaptive mesh refinement is used, this type of error estimator does give a reasonable estimation of the true error if a correction factor is provided, as indeed shown in previous papers. This corresponds to the phenomenon found in Part 1 of the paper where we noted that the global L_2 projection is more effective on non-uniform meshes.

4. CONCLUDING REMARKS

As expected, the superconvergent recovery procedure described in Part 1 of the paper leads by virtue of its properties to an accurate form of Z^2 error estimator with demonstrably good effectivity indices. Indeed, the originally used global L_2 projection process or its alternatives should now be abandoned as the cost of the new recovery procedure now proposed is generally less and its results more accurate. We must remark, however, that these alternatives which were used previously in the error estimation did not lead to wrong adaptive refinement. As we have found from the presented examples, the corresponding error estimates did provide a good indication of the distribution of the actual error and indeed the quality of the estimation improves as the energy norm error becomes equally distributed.

We have now shown that with the recovered superconvergent solution the pointwise error of the finite element solution can be accurately estimated. Although the control of such local errors is not as simple as the procedure for ensuring a specified overall energy norm error, it is desirable that the estimates should be included in the results of any finite element analysis.

Two further points need to be mentioned and both are motived by the excellent recovery characteristics of the new procedure here discussed.

The first is the fact that the error estimations given here refer to the errors in the original finite element solution (σ_h) and not to the recovered solution σ^* which, as we demonstrated, is very much more accurate.

The second is that we have concentrated here on error norms involving the derivatives (σ) and not the basic function u (such as displacement).

Is there a possibility of extending the range of error estimation to cover these problems? Clearly, this is a direction of future research and some possibilities are now being investigated.

REFERENCES

1. O. C. Zienkiewicz and J. Z. Zhu, 'The superconvergent patch recovery and *a posteriori* error estimates. Part 1: The recovery technique'. *Int. j. numer. methods eng.*, **33**, 1331–1364 (1992)
2. O. C. Zienkiewicz and J. Z. Zhu, 'A simple error estimator and adaptive procedure for practical engineering analysis', *Int. j. numer. methods eng.*, **24**, 337–357 (1987).
3. I. Babuska and W. C. Rheinboldt, 'Error estimates for adaptive finite element computations', *SIAM J. Numer. Anal.*, **15**, 736–753 (1978).
4. D. W. Kelly, J. P. R. Gago, O. C. Zienkiewicz and I. Babuska, 'A posteriori error analysis and adaptive processes in the finite element method, Part I—error analysis', *Int. j. numer. methods eng.*, **19**, 1593–1619 (1983).
5. J. P. R. Gago, D. W. Kelly, O. C. Zienkiewicz and I. Babuska, 'A posteriori error analysis and adaptive processes in the finite element method, Part II—adaptive mesh refinement', *Int. j. numer. methods eng.*, **19**, 1621–1656 (1983).
6. O. C. Zienkiewicz, J. P. R. Gago and D. W. Kelly, 'The hierarchic concept in finite element analysis', *Comp. Struct.*, **16**, 53–65 (1983).
7. R. E. Bank and A Weiser, 'Some *a posteriori* error estimators for elliptic partial differential equations', *Math. Comp.*, **44**, 283–301 (1985).
8. J. T. Oden, L. Demkowicz, W. Rachowicz and T. A. Westermann, 'Toward a universal *h–p* adaptive finite element strategy, Part 2. *A posteriori* error estimation', *Comp. Methods Appl. Mech. Eng.*, **77**, 113–180 (1989).
9. O. C. Zienkiewicz and J. Z. Zhu, 'Error estimates and adaptive refinement for plate bending problems', *Int. j. numer. methods eng.*, **28**, 2839–2853 (1989).
10. O. C. Zienkiewicz, Y. C. Liu and G. C. Huang, 'Error estimation and adaptivity in flow formulation for forming problem', *Int. j. numer. methods eng.*, **25**, 23–42 (1988).
11. O. C. Zienkiewicz, Y. C. Liu and G. C. Huang, 'Error estimates and convergence rates for various incompressible elements', *Int. j. numer. methods eng.*, **28**, 2191–2202 (1989).
12. J. Wu, J. Z. Zhu, J. Szmelter and O. C. Zienkiewicz, 'Error estimation and adaptivity in Navier Stokes incompressible flows', *Comp. Mech.*, **6**, 259–270 (1990).
13. J. Z. Zhu and O. C. Zienkiewicz, 'Superconvergence recovery technique and *a posteriori* error estimators', *Int. j. numer. methods eng.*, **30**, 1321–1339 (1990).
14. O. C. Zienkiewicz and J. Z. Zhu, 'The three R's of engineering analysis and error estimation and adaptivity', *Comp. Methods Appl. Mech. Eng.*, **82**, 95–113 (1990).
15. O. C. Zienkiewicz and J. Z. Zhu, 'Adaptivity and mesh generation', *Int. j. numer. methods eng.*, **32**, 783–810(1991).
16. O. C. Zienkiewicz, J. Z. Zhu and N. G. Gong, 'Effective and practical *h–p* adaptive analysis procedures for the finite element method', *Int. j. numer. methods eng.*, **28**, 879–891 (1989).
17. E. Hinton and J. S. Campbell, 'Local and global smoothing of discontinuous finite element functions using a least square method', *Int. j. numer. methods eng.*, **8**, 461–480 (1974).